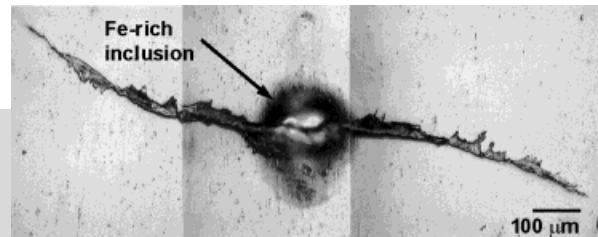


Mechanical Behavior of Particle Reinforced Metal Matrix Composites**

By Nikhilesh Chawla,* and Yu-Lin Shen

Metal matrix composites provide significantly enhanced properties — like higher strength, stiffness and weight savings — in comparison to conventional monolithic materials. Particle reinforced MMCs are attractive due to their cost-effectiveness, isotropic properties, and their ability to be processed using similar technology used for monolithic materials. This review captures the salient features of experimental as well as analytical and computational characterization of the mechanical behavior of MMCs. The main focus is on wrought particulate reinforced light alloy matrix systems, with a particular emphasis on tensile, creep, and fatigue behavior.



1. Introduction

Metal matrix composites (MMCs), like most composite materials, provide significantly enhanced properties over conventional monolithic materials, such as higher strength, stiffness, and weight savings.^[1-4] While continuous fiber reinforcement provides the most effective strengthening (in a given direction), particle reinforced materials are more attractive due to their cost-effectiveness, isotropic properties, and their ability to be processed using similar technology used for monolithic materials. A large amount of work has been conducted in an effort to characterize the mechanical behavior of particle reinforced metal matrix composites. In this review, we attempt to capture the salient features of experimental as well as analytical and computational characterization of the mechanical behavior of MMCs. We restrict ourselves to wrought particulate reinforced light alloy matrix systems, with a particular emphasis on tensile, creep, and fatigue behavior.

2. Strengthening Mechanisms in Metal Matrix Composites

The strengthening mechanisms observed in MMCs may be divided into two categories, direct and indirect strengthening. Direct strengthening in particulate reinforced metals is an extension of the classical composite strengthening mecha-

nisms used to describe the behavior of continuous fiber reinforced composites.^[1,5,6] Under an applied load, the load is transferred from the weaker matrix, across the matrix/reinforcement interface, to the typically higher stiffness reinforcement. In this manner, strengthening takes place by the reinforcement “carrying” much of the applied load. Due to the lower aspect ratio of particulate materials, load transfer is not as efficient as in the case of continuous fiber reinforcement, but is still significant in providing strengthening.^[7-9]

[*] Prof. N. Chawla
Materials Science and Eng. Program
Department of Chemical and Materials Eng.
Arizona State University
P.O.Box 876006
Tempe, AZ 85287-6006 (USA)
E-mail: nchawla@asu.edu
Prof. Y.-L. Shen
Department of Mechanical Engineering
University of New Mexico
Albuquerque, NM 87131 (USA)

[**] NC acknowledges continued research support from The United States Automotive Materials Partnership (USAMP) through the Department of Energy, and the office of Naval Research (Dr. A. K. Vasudruan, Program Manager), under contract # N 00014-01-1-0694. YLS acknowledges the support from the University of New Mexico Regents' Lectureship.

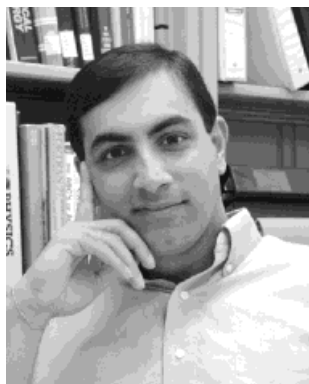
In metal matrix composites, where a high stiffness ceramic reinforcement is embedded in a metallic alloy, the thermal mismatch between the high expansion metallic matrix and the low expansion ceramic is typically quite high. Thus, upon cooling, dislocations form at the reinforcement/matrix interface due to the thermal mismatch. In this manner, thermally-induced dislocation punching results in "indirect strengthening" of the matrix.^[10-13] In age-hardenable matrix materials, the thermally-induced dislocations (formed upon quenching from the solution treatment) serve as heterogeneous nucleation sites for precipitate formation during the aging treatment.^[14] Not only is there a preferential distribution of precipitates in the particle/matrix interface region, but the higher density of dislocations also causes an acceleration in the time to peak-aging compared to the unreinforced alloy of a similar composition. An increase in reinforcement volume fraction or a decrease in particle size increases the amount of indirect strengthening, since a larger amount of interfacial area exists for dislocation punching to take place.

The extent of indirect strengthening is more difficult to quantify than the contribution from direct strengthening. Krajewski et al.^[15] used a thermomechanical treatment, consisting of solution treating, rolling, followed by aging (T8 treatment) to provide a homogeneous distribution of dislocations (and subsequently precipitates) in both the matrix of the composite and the unreinforced alloy. In this manner, the difference in strengthening between unreinforced and composite could be attributed primarily to load transfer to the reinforcement. Chawla et al.^[9] compared experimental data on

T8-matrix composites with a simple modified shear lag analysis proposed by Nardone and Prewo,^[7] and obtained extremely good correlation. It was also shown that in peak-aged materials only (without rolling), the strengthening in the composite could be partitioned into direct and indirect strengthening components.

3. Tensile Behavior

In metal matrix composites, the reinforcing phase typically is much stiffer than the matrix. Thus, as described above, a significant fraction of the stress is initially borne by the reinforcement. Microplasticity takes place in MMCs, at a fairly low stress, which corresponds to a slight deviation from linearity in the stress-strain curve. This point is termed the proportional limit stress. Microplasticity in the composites has been attributed to stress concentrations in the matrix at the poles of the reinforcement and/or at sharp corners of the reinforcing particles.^[16-18] The initial microyielding stress decreases with increasing volume fraction, as the number of stress concentrating points increases.^[18] The incorporation of particles in the matrix so results in an increase in "apparent work hardening" in the material. The term "apparent" is used here because the higher observed work hardening rate is a simple function of lower matrix volume (by incorporation of the particles) and not necessarily due to a change in work hardening mechanisms. Thus, the higher work hardening rate observed in the composites is due to geometric constraints imposed by the presence of the reinforcement. When



Nikhilesh Chawla is currently Assistant Professor and Graduate Chair in the Department of Chemical and Materials Engineering at Arizona State University. He received his Ph.D. from the University of Michigan in 1997. He was a postdoctoral fellow jointly at Ford Motor Co. and the University of Michigan, and a senior development engineer at Hoeganaes Corp. prior to joining Arizona State University in 2000. Prof. Chawla's research interests include the mechanical behavior of advanced materials at bulk and small length scales, including metal matrix composites, Pb-free solders, and powder metallurgy materials. He has authored or co-authored close to 40 publications and is the recipient of a National Science Foundation Early Career Development Award (2001) and The Office of Naval Research Young Investigator Award (2001).



Yu-Lin Shen is currently Assistant Professor and Regents' Lecturer in the Department of Mechanical Engineering at the University of New Mexico. He received his Ph.D. in Engineering from Brown University in 1994. He was a post-doctoral research associate at Massachusetts Institute of Technology before joining The University of New Mexico in 1996. Prof. Shen's research interest encompasses materials and mechanics, with particular attention devoted to the thermo-mechanical behavior of materials. Currently his main effort is in the areas of materials modeling, metal matrix composites, and structural integrity of microelectronic devices and packages. He has published more than thirty-five papers in international journals.

the matrix is significantly work hardened, the matrix is placed under great constraint with an inability for strain relaxation to take place. This causes the onset of void nucleation and propagation, which take place at a lower far field applied strain than that observed in the unreinforced material.

Figure 1 shows the tensile behavior of an Al-Cu-Mg (2080)/SiC_p-T8^[121] composite with varying volume fraction (at a constant particle size of 5 μm) and varying particle size (at a constant volume fraction of 20%). The microstructure was maintained relatively constant by introducing a T8 treatment to all composites. With an increase in volume fraction, higher elastic modulus, macroscopic yield and tensile strengths were observed, coupled with lower ductility (Fig. 1a). With increasing volume fraction, more load is transferred to the reinforcement which also results in a higher ultimate tensile strength. The work hardening rate increases with increasing volume fraction of reinforcement (and decreasing matrix volume). The lower ductility can be attributed to the earlier onset of void nucleation with increasing amount of reinforcement. It should be noted that cracked particles in the composite, which may result from processing of composites with fairly coarse particulate reinforcement, do not contribute to load transfer or strengthening and would decrease strength. The high stress concentration at the tips of the cracked particles would also contribute to a lower ductility in the composite, compared to the unreinforced alloy.

The effect of particle size on tensile behavior, documented by several investigators,^[19-21] indicates an increase in ductility with a decrease in particle size (Fig. 1b). This may be attributed to an increase in the SiC particle strength with a decrease in particle size, because the probability of a strength-limiting flaw existing in the volume of the material decreases. At relatively large particle sizes of this material, e.g., above 20 μm, a significant amount of particle cracking takes place during extrusion prior to testing. Cracked particles do not carry any load effectively and can be effectively thought of as voids, so the strength is lower than that of the unreinforced material. It has also been proposed, however, that because of the higher plastic constraint imposed by the lower interparticle spacing, that the nucleated voids are unable to coalesce as easily.^[20] A higher work hardening rate has also been observed with decreasing particle size.^[21,22] This is attributed to the formation of dislocation tangles around the particles, due to plastic incompatibility between the reinforcement and matrix, and the formation of a dislocation cell structure with a cell size inversely proportional to the interparticle spacing.^[23] The tensile fracture surface of a particulate reinforced composite shows quite a contrast between the dimpled nature of fracture in the matrix coupled with brittle fracture of the SiC particles (Fig. 2).^[24] Notice that the particle/matrix interface remains intact, indicating that the shear strength at the interface was higher than the particle fracture strength.

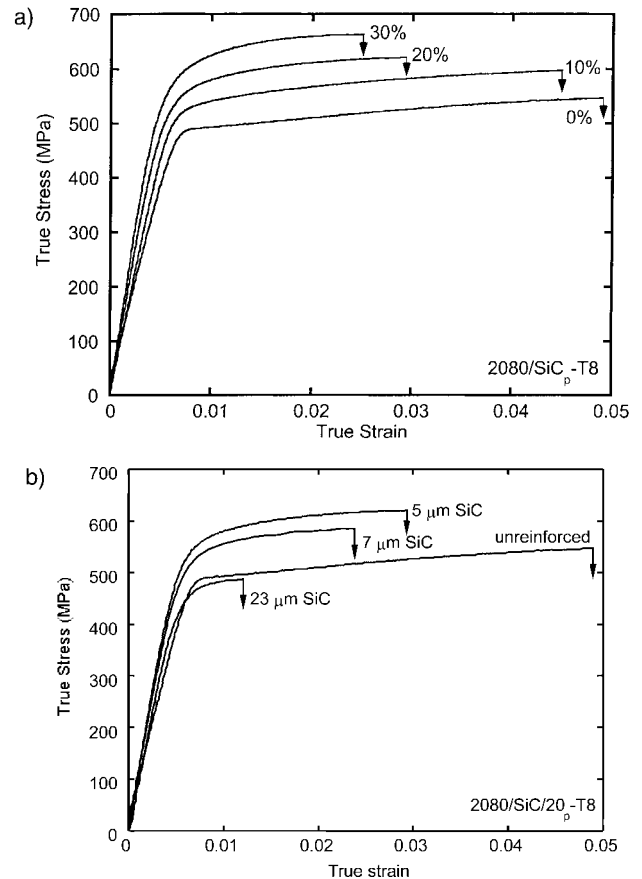


Fig. 1. Tensile behavior of an Al-Cu-Mg (2080)/SiC_p-T8 composite with: a) varying volume fraction (at a constant particle size of 5 μm) and b) varying particle size (at a constant volume fraction of 20%).

4. Creep Behavior

In general, the addition of a high stiffness reinforcement greatly increases the creep resistance over the unreinforced alloy.^[25,26] Nieh^[26] studied the creep behavior of 6061/SiC/20_p and 6061/SiC/20_w, and compared it to the unreinforced 6061 alloy (Fig. 3). A much higher creep resistance was obtained in the composite with an accompanying higher sensitivity to applied stress (much higher stress exponent *n*). An enhanced creep resistance was also obtained with the higher aspect ratio whiskers than with particles, presumably due to

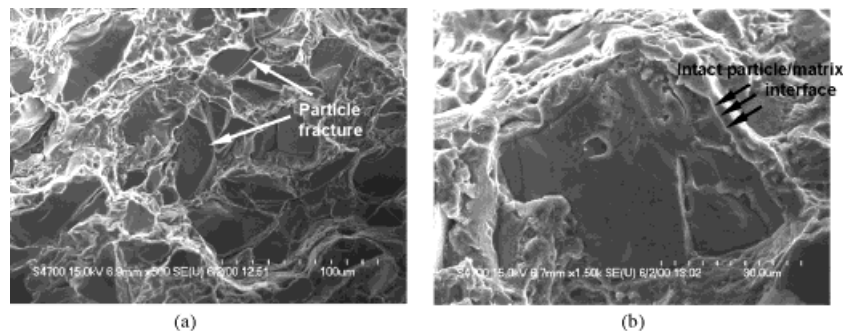


Fig. 2. Tensile fracture surface of a particulate reinforced composite showing dimpled fracture in the matrix coupled with brittle fracture of the SiC particles.

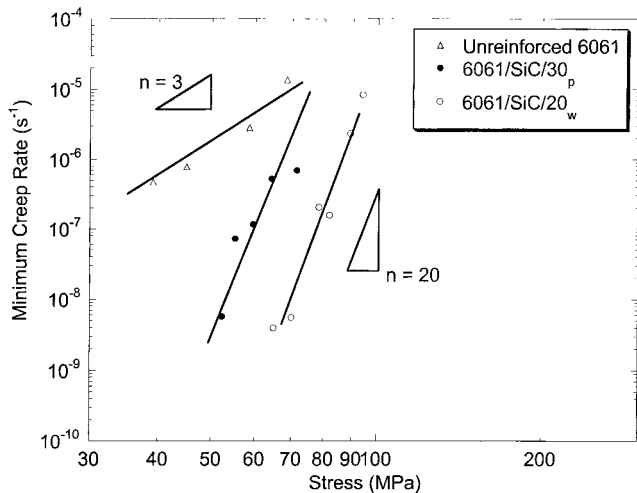


Fig. 3. Creep behavior of particle and whisker reinforced composites.^[26] Notice the higher creep resistance of the whisker reinforced material, due to more effective load transfer to the reinforcement.

more effective load transfer from the matrix to the high stiffness reinforcement. Webster^[27] also characterized the creep behavior of the matrix alloy and its whisker reinforced composite with increasing temperature. It was observed that at intermediate temperatures (500–720 K) the strength is controlled by the whiskers, as the load is transferred to the high modulus and aspect ratio reinforcement. The strength becomes matrix-controlled at very high temperatures (720–900 K), perhaps due to increasingly lower interfacial shear strength and lower efficiency in load transfer to the whisker reinforcement.

Anomalously high values of the activation energy, Q , and stress exponent, n , have been reported in MMCs.^[25,26,28–30] Nardone and Strife^[28] rationalized this by proposing the concept of a threshold stress σ_r , for creep deformation, originally used to explain the high values for Q and n in dispersion-strengthened alloys.^[31–33] By introducing the threshold stress, the general steady-state creep rate is modified to:

$$\dot{\epsilon}_{ss} = A \left(\frac{\sigma - \sigma_r}{E} \right)^n \exp \left(\frac{-Q}{RT} \right) \quad (1)$$

where A is a constant, E is the elastic modulus of the composite, and Q is the activation energy. The latter two variables are corrected for temperature dependence. The physical explanation for the threshold stress in the discontinuously reinforced composite system can be attributed to a variety of reasons:^[29] (1) Orowan bowing between particles, (2) back-stress associated with dislocation climb, (3) attractive force between dislocations and particles, resulting from relaxation of the strain field of dislocations at the particle/matrix interface.^[34] Due to the higher apparent work hardening rate, i.e., lower volume of matrix material, the enhancement of dislocation/dislocation interactions can contribute to σ_r , although this mechanism is more plausible at ambient temperature.

Load transfer to the reinforcement, despite the lower aspect ratios of particles and whiskers, is significant, as the

applied load is carried by the high stiffness reinforcement. With increasing load transfer to the reinforcement, the resolved shear stress on dislocations in the matrix may be lowered significantly below that required for Orowan bowing. It has also been observed that below a critical strain rate diffusional relaxation around the SiC particles is the rate-controlling mechanism, while above this point, a greater degree of load is carried by the high stiffness particles.^[35] In addition to the threshold stress, additional proposed mechanisms for the anomalously high values of Q and n include power law break-down of the matrix^[36,37] and interfacial decohesion at the particle/matrix interface.^[38] The reinforcement may contribute to changes in the matrix during creep by localized recrystallization at corners or interfaces and precipitate coarsening at the particle/matrix interface, where the density of precipitates is the highest (because of the dislocation defects being higher at the interface).

It has been shown that in powder processed composite materials, oxide dispersions (not present in the unreinforced alloy) may also contribute to extremely high “anomalous” values of n and Q .^[39,40] Park et al.^[39] suggested that the presence of fine oxide particles, incoherent with the matrix, arising from the powder metallurgy process used to fabricate the composite, served as effective barriers for dislocation motion and gave rise to a threshold creep stress. The high creep stress exponent and increase in exponent with decreasing applied stress were attributed to the oxide particles in the matrix. Li and Langdon^[40] support this conclusion, and add that in ingot metallurgy composites, compared with powder metallurgy-processed composites of the same composition, viscous glide is the rate-controlling mechanism because of the absence of oxide particles.

Li and Langdon^[41] also proposed two separate classes of creep behavior in metal matrix composites. In class M (pure metal type) materials dislocation climb is the rate-controlling mechanism, with a stress exponent of around 5 and an activation energy similar to the value for self-diffusion in the matrix. In class A (alloy type) metals, viscous dislocation glide is the rate-controlling mechanism, with a stress exponent of around 3 and an activation energy associated with the viscous drag of the solute atmospheres. Exceptionally high creep rates were observed at the highest stress levels, perhaps due to dislocations breaking away from solute atom atmospheres.^[41] It should be noted that in unreinforced solid solution alloys a transition exists between class M behavior at low stresses to class A behavior at higher stresses.^[42]

5. Fatigue Behavior

Much of the driving force for development of MMCs has been that monolithic lightweight alloys have inadequate fatigue resistance for many demanding applications. The use of a high stiffness ceramic reinforcement in particulate form, such as SiC, can result in a substantial increase in fatigue resistance while maintaining cost at an acceptable level. This is an impor-

tant design criterion in many applications, e.g. in automotive components. The fatigue resistance of particulate MMCs depends on a variety of factors, including reinforcement particle volume fraction, particle size, matrix microstructure, the presence of inclusions or defects that arise from processing, and testing environment.^[43–45] The effect of these factors on the fatigue behavior of particle reinforced MMCs is summarized in this section. Here we concentrate on stress versus cycles (S-N) fatigue behavior. A Paris Law approach, i.e., measuring fatigue crack growth versus stress intensity at the crack tip, has also been used extensively by several investigators.^[46–49]

Several studies have shown that increasing volume fraction and decreasing particle size both result in enhanced fatigue resistance.^[19,50] In the composite, most of the load is carried by the high modulus, high strength reinforcement, so for a given stress, the composite undergoes a lower average strain than the unreinforced alloy. Thus, the fatigue lives of particle reinforced metal matrix composites are generally longer than those of unreinforced metals (Fig. 4). These improvements are most pronounced at lower stresses, in the high cycle fatigue regime, while at high stress the differences between reinforced and unreinforced materials are reduced. This can be attributed to "ductility exhaustion" of the composites in the low cycle fatigue regime. With decreasing particle size, for a given reinforcement volume fraction, the reinforcement interparticle spacing decreases, resulting in more barriers for the reversible slip motion that takes place during fatigue, and a decrease in strain localization by cyclic slip refinement. Above a critical particle size, reinforcement fracture is predominant and contributes to premature fatigue life, because of the increased propensity for particle cracking as the particle size increases.^[19] Narrowing of the particle size range distribution also results in higher fatigue life, particularly when eliminating larger particles that are more prone to cracking.^[51]

In addition to particle reinforcement, the matrix microstructure also significantly influences the fatigue behavior of

the composite. Factors affecting the matrix microstructure include size, shape, and spacing of precipitates, grain size, and non-reinforcement dispersoids or inclusions (such as Fe-rich inclusions that are formed during processing). The effect of grain size has not been explicitly examined, but composites follow the same trend as monolithic materials, i.e., for a given matrix alloy composition and volume fraction of reinforcement, finer grain sizes generally result in improved properties.

Contrary to conventional wisdom for monolithic materials, in MMCs high matrix yield and ultimate tensile strength do not necessarily reflect high fatigue strength (defined here as fatigue runout at 10^7 cycles). Vyletel et al.^[52] showed that there was no significant difference in fatigue behavior between naturally aged and artificially aged MMC, even though the naturally aged material had a much lower yield and ultimate strength. Chawla et al.^[9] compared two materials with constant reinforcement volume fraction and particle size, but very different microstructures. A thermomechanical treatment (T8) of the Al-Cu-Mg alloy produced a fine and homogeneous distribution of S' precipitates, while a thermal treatment only (T6) resulted in coarser and inhomogeneously distributed S' precipitates. Because of finer and more closely spaced precipitates, the composite that underwent a T8 treatment exhibited higher yield strengths than the T6 materials. Despite its lower yield strength, however, the T6 matrix composites exhibited higher fatigue resistance than the T8 matrix composites. This contrasting behavior between monotonic and cyclic loading can be attributed to the strong influence of the presence, stability, and morphology of the S' precipitates in the matrix of the composite.^[53–55] In fatigue, failure processes are affected by a variety of microstructural factors, which include resistance to dislocation motion and pileup at precipitates and/or reinforcement particles and cracking along slip bands. Throughout the fatigue process, dislocations either cut precipitates or loop around them during cyclic deformation, depending on precipitate coherency and size.^[53,54] In the T8 materials, the precipitates are fine enough that it is believed that the precipitates are cut by dislocations and localized slip takes place, which reduces the strengthening effect of precipitates, thereby impairing the fatigue strength. In the T6 materials, the larger precipitate size allows them to retain their precipitates structure and strength during fatigue.

Overaging heat treatments also modify the matrix microstructure, resulting in coarsening of the precipitate structure, while retaining a homogeneous precipitate distribution, which directly influences fatigue life.^[9] Figure 5a shows the coarsening and increase in precipitate spacing in the matrix of MMCs overaged at various temperatures for 24 hours. Increasing precipitate spacing decreases both fatigue strength and fatigue lifetime (Fig. 5b). This is to be expected since coarser precipitates result in a larger interprecipitate spacing and easier bypass of dislocations. For the composites subjected to higher overaging temperatures, the yield strength

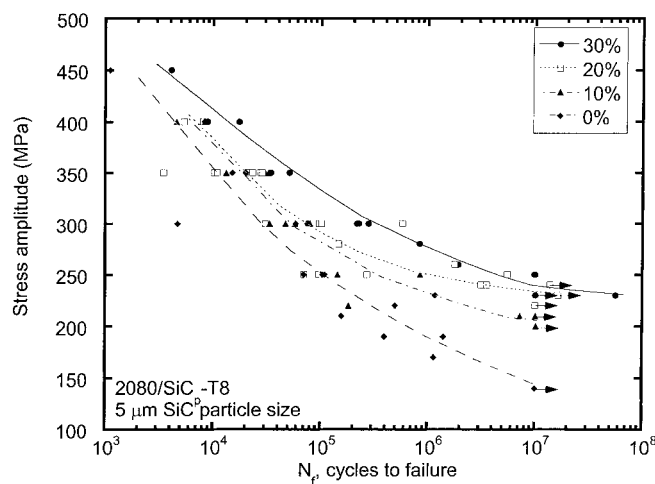


Fig. 4. Effect of reinforcement volume fraction ($5 \mu\text{m SiC}$ particle size,) on fatigue life of a $2080/\text{SiC}_p$ composite. Increasing volume fraction of the reinforcement results in enhanced fatigue resistance.

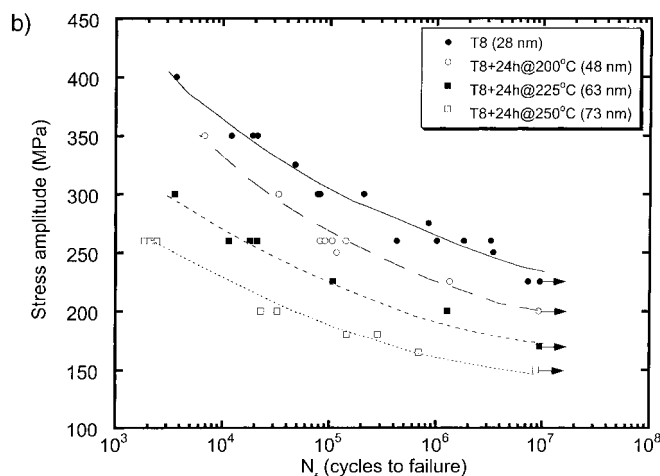
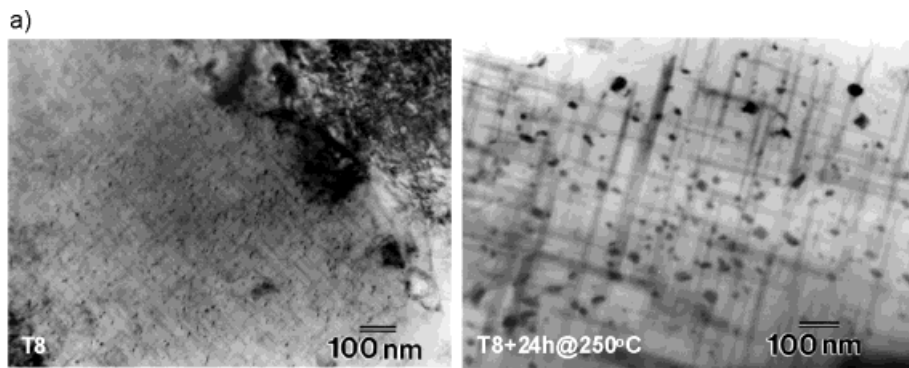


Fig. 5. Effect of overaging on: a) Microstructure. Precipitate coarsening and increase in precipitate spacing in MMCs is observed; and b) Fatigue life. Increasing precipitate spacing decreases both fatigue strength and fatigue lifetime (precipitate spacings are given in parentheses).

and fatigue strength also decrease with increasing precipitate spacing. It should be mentioned that precipitate size alone should not be taken as the determining factor for fatigue resistance. Rather, the precipitates should be of sufficient size to not be susceptible to precipitate shearing, but semi- or completely coherent with the matrix to impose repulsive stress fields against dislocation motion.

Processing-related defects in the form of intermetallic inclusions or particle clusters are also part of the matrix microstructure, and play a role in fatigue strength, particularly in powder metallurgy processed materials.^[19,56] These defects act as stress concentrators that increase the local stress intensity in the material and promote easy crack nucleation. It has been shown that crack initiation during fatigue takes place at these defects, which are typically located at the surface of the specimen.^[57] This is because inclusions at the surface are more highly stressed than inclusions completely within the matrix (where more load is borne by the reinforcement), so a higher stress concentration and, thus, higher probability for crack initiation is present at the surface. For a given inclusion size, the stress concentration in a composite where the inclusion is surrounded by high stiffness reinforcement particles, is lower than in the unreinforced alloy. Since more of the load is being “shared” by the high stiffness SiC particles in the composite, an inclusion in the composite will be subjected to

lower stress than a similar inclusion in the unreinforced alloy. In extruded materials, the overall size of inclusions is also lower in composites since the ceramic reinforcement particles break the brittle inclusions into smaller sizes during extrusion.

It is interesting to note that in the low cycle regime, cracks seem to originate relatively early in fatigue life (around 10% of total life).^[19,58] In the high cycle regime, on the other hand, crack initiation can occur quite late (after about 70–90% of the life of the specimen). While crack growth is relatively unimpeded in unreinforced materials (Fig. 6a), crack growth is hindered by mechanisms such as crack deflection and crack trapping in the composite (Fig. 6b).^[59]

Several MMC applications will require fatigue resistance at elevated temperatures (on the order of 150–175 °C). Figure 7 shows the elevated temperature fatigue performance of MMCs in comparison with the room temperature data shown in Figure 4.^[60] The most significant debit in fatigue strength occurred between 25 and 150 °C. The incremental increase in temperature to 170 °C resulted in a

modest decrease in fatigue strength. In applications where elevated temperature fatigue resistance is a criterion, the temperature at which the composite is aged becomes very impor-

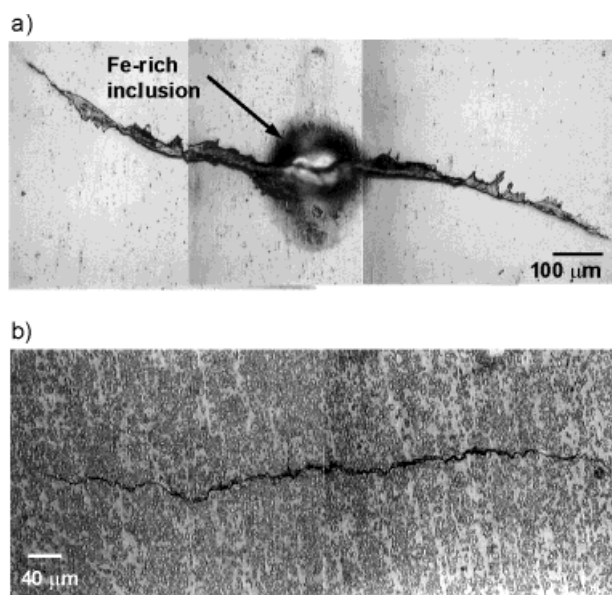


Fig. 6. Fatigue crack initiation and growth in a) unreinforced 2080 Al and b) in 2080/SiC_p composite. Notice that crack growth is hindered by mechanisms such as crack deflection and crack trapping in the composite.

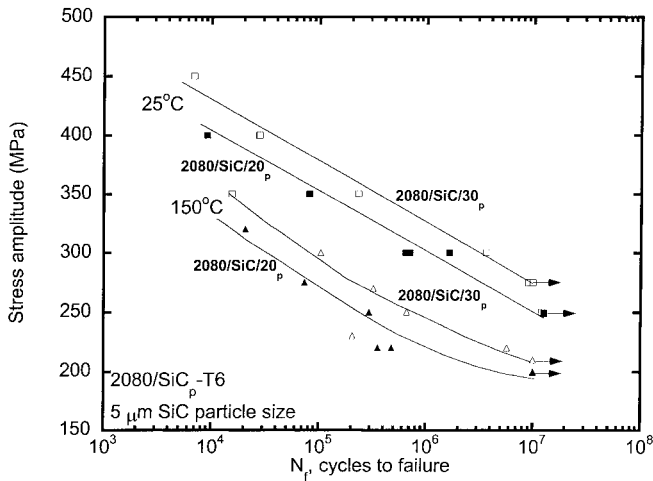


Fig. 7. Elevated temperature fatigue performance of an MMC in comparison with the room temperature data shown in Figure 4.

tant. At slightly higher temperatures than the aging temperature, a severe decrease in fatigue strength may take place because of significant matrix overaging. The fatigue strength in the composites seems to be directly proportional to the strength of the matrix, although the decrease in fatigue strength due to temperature is significantly higher than the decrease in yield strength. This may be caused by changes in matrix microstructure and decrease in matrix strength from a combination of long-term exposure and cyclic stress at elevated temperatures.

6. Modeling of Mechanical Behavior

Analytical and numerical modeling of MMCs provide an effective means of (a) predicting effective properties of the composite (e.g., Young's modulus) from the known properties of its constituents and (b) revealing deformation and damage characteristics. In particle reinforced metal matrix composites, numerical modeling is often more effective than analytical modeling since the composites lack the structural simplicity of continuous fiber composites or laminates and hence are not readily amenable to closed-form theoretical analyses. In the following sections, we discuss the prediction of effective properties, deformation characteristics, and damage related issues.

7. Prediction of Effective Properties

The mechanical properties of a particle reinforced MMCs are dependent on factors such as reinforcement volume fraction, shape, contiguity, and spatial distribution within the matrix. Although it is a very complex problem, various methods have been proposed to estimate the overall elastoplastic response as well as the bounds for effective elastic moduli of the composite. Comprehensive reviews of the literature can be found in references.^[61-67] Here we briefly discuss selected

analytical models that predict the effective modulus of the composite.

Hashin and Shtrikman^[68] proposed upper and lower bounds for an isotropic aggregate based on variational principles of linear elasticity:

$$K^{\text{upper}} = K_R + (1 - f) \left[\frac{1}{K_M - K_R} + \frac{3f}{3K_R + 4\mu_R} \right]^{-1} \quad (2)$$

$$K^{\text{lower}} = K_M + f \left[\frac{1}{K_R - K_M} + \frac{3(1-f)}{3K_M + 4\mu_M} \right]^{-1} \quad (3)$$

$$\mu^{\text{upper}} = \mu_R + (1 - f) \left[\frac{1}{\mu_M - \mu_R} + \frac{6f(K_R + 2\mu_R)}{5\mu_R(3K_R + 4\mu_R)} \right]^{-1} \quad (4)$$

$$\mu^{\text{lower}} = \mu_M + f \left[\frac{1}{\mu_R - \mu_M} + \frac{6(1-f)(K_M + 2\mu_M)}{5\mu_M(3K_M + 4\mu_M)} \right]^{-1} \quad (5)$$

where K and μ are the bulk and shear moduli, respectively, and f is the volume fraction of reinforcing particles. The superscripts "upper," "lower," "M," and "R" refer to the upper and lower bound estimates, and matrix and reinforcement, respectively. Given the moduli of the matrix and reinforcement, the overall bounds of Young's modulus are then obtained by Equations 2-5 and the following relation between E , K , and μ :

$$E = \frac{9K}{1 + 3K/\mu} \quad (6)$$

Eshelby^[69] treated the three-dimensional elasticity problem of a single ellipsoidal inclusion in an infinite matrix. This approach has been employed quite extensively in modified forms in the analyses of discontinuously reinforced composite materials.^[70-76] Mura^[70] provided estimates for finite concentrations of reinforcements. Taking the reinforcement geometry to be spherical, the Mura expressions for the effective moduli are

$$\mu = \mu_M \left[1 + f(\mu_M - \mu_R) / \left\{ \mu_M + 2(\mu_R - \mu_M) \frac{4 - 5\nu_M}{15(1 - \nu_M)} \right\} \right]^{-1} \quad (7)$$

$$K = K_M \left[1 + f(K_M - K_R) / \left\{ K_M + \frac{1}{3}(K_R - K_M) \frac{1 + \nu_M}{1 - \nu_M} \right\} \right]^{-1} \quad (8)$$

where ν is the Poisson's ratio. The composite Young's modulus is then obtained from Equation 6. The results based on this approach are only valid for relatively small volume fractions (smaller than about 0.25) of reinforcing particles.

The effective Young's modulus of composites with spherical reinforcements, with a large volume fraction (greater than 0.5), can be predicted by a self-consistent method proposed by Kroner^[71] and Budiansky.^[72] This method is also based on Eshelby's equivalent inclusion model, but assumes that the moduli of the infinite medium are equal to the overall moduli of the composite. For spherical inclusions, Budiansky's self-consistent relation is given by^[72]

$$\mu = \mu_M + \frac{f\mu(\mu_R - \mu_M)}{\mu + 2(\mu_R - \mu)(4 - 5\nu)\{15(1 - \nu)\}^{-1}} \quad (9)$$

$$K = K_M + \frac{fK(K_R - K_M)}{K + \frac{1}{3}(K_R - K)(1 + \nu)\{1 - \nu\}^{-1}} \quad (10)$$

Solutions are obtained by setting

$$\nu = \frac{3K - 2\mu}{2(\mu + 3K)} \quad (11)$$

and solving Equations 9 and 10 simultaneously. Once again, the composite Young's modulus is then obtained by Equation 6.

As an alternative to analytical modeling, numerical techniques such as finite element analysis have become increasingly more popular, where the geometry of the components, thermomechanical history of the composite, are incorporated into the simulation of the mechanical properties. One common approach is to use a unit-cell model, where one or more reinforcement particles are embedded within the Al matrix, to simulate a composite material with a periodic array of reinforcement. Examples of unit-cell models are shown in Figure 8, in which the left vertical boundary represents the axially symmetric axis and mirror symmetry exists about the bottom boundary. A periodic arrangement of particles with the shape of a "unit cylinder", "truncated cylinder", "double-cone" and "sphere" (Figs. 8a, b, c and d, respectively) may be simulated using the appropriate boundary conditions.^[77] It should be noted that in actual composites the particles commonly contain sharp corners, so spherical particles are not necessarily a realistic choice for simulation. Object oriented

finite element techniques have been employed that are able to incorporate the "true" composite microstructures, that take into consideration particle morphology and clustering of particles, as a basis for analysis using finite element techniques.^[78]

Numerical predictions of the effective Young's modulus for an Al/SiC_p composite are shown in Figure 9, where the composite Young's modulus (normalized by the Young's modulus of the matrix) for unit cylinder and spherical reinforcement are plotted as a function of reinforcement volume concentration and compared with analytical predictions. The

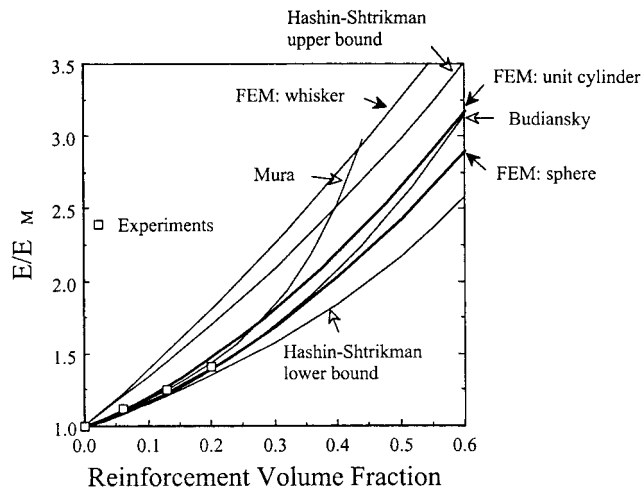


Fig. 9. Comparisons of the variation of effective Young's modulus (normalized by Young's modulus of the unreinforced matrix) as a function of reinforcement volume fraction among the numerical and analytical results. (Matrix: Al-3.5 Cu alloy; reinforcement: SiC particles.) Experimental points are shown as squares.

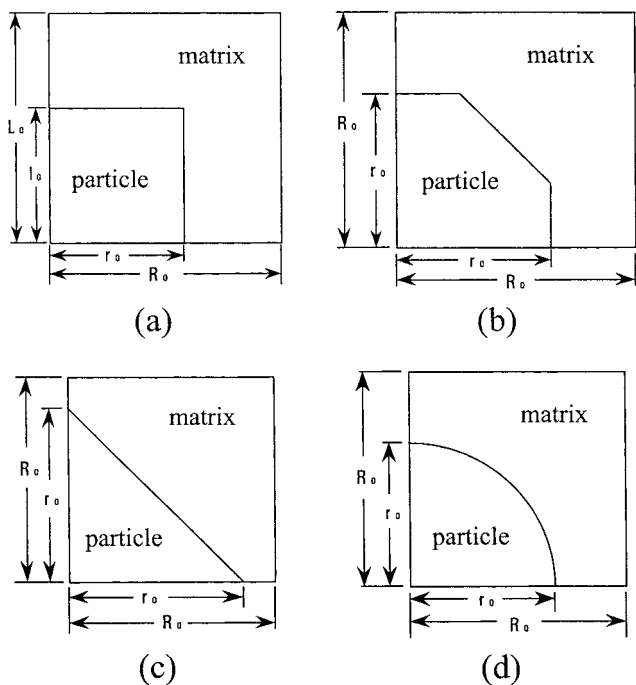


Fig. 8. Types of unit cells used for simulating different reinforcement shapes in a composite: a) unit cylinder, b) truncated cylinder, c) double-cone and d) sphere. The left boundaries represent the axially symmetric axes.

unit cylinder particle has a greater stiffening effect than the spherical particle. Clearly, load transfer by a shear-lag type of mechanism is more effective across a planar interface than a spherical interface. Both numerical curves fall within the Hashin-Shtrikman bounds described by Equations 2–5. Mura's model, Equations 7 and 8, matches the numerical prediction for spherical particles well when the reinforcement fraction is small, but a significant deviation occurs at larger reinforcement fractions, as discussed above. The predictions of the self-consistent method by Budiansky, Equations 9 and 10, match the numerical predictions for spherical particles very closely for a reinforcement fraction less than about 0.35. Above this volume fraction, this method predicts a stiffer response with the spherical reinforcement than the finite element method. The numerical predictions show fairly good agreement with experimental results on the effective elastic moduli obtained for a Al-3.5Cu alloy reinforced with 0, 6, 13 and 20 vol. % SiC particles,^[79] which are also shown in Figure 9. Although the SiC particles in actual materials contain sharp corners, the experimental values are slightly lower than the numerical predictions for unit cylinders. This may be attributed to some degree of particle fracture during thermo-mechanical processing, development of residual stresses, and particle clustering in the composite.^[80] The results shown in

Figure 9 clearly indicate that a simple rule-of-mixtures approach is not valid in estimating the effective modulus of particle reinforced MMCs. The rule-of-mixtures approach is based on the condition of isostrain between matrix and reinforcement, and hence is valid only for continuous fiber reinforcement with high aspect ratios.

Similar numerical approaches to that described above can be used to model the overall *inelastic* response of the composite. Characterizing the matrix as an isotropically hardening elastic-plastic solid (following the experimental stress-strain curve of a peak-aged Al-3.5Cu alloy) and the SiC particles as an elastic solid, the calculated tensile stress-strain response of Al/SiC/20_p composites, having the four particle shapes described above, are shown in Figure 10. Clearly, particle shape has a significant influence on the overall tensile behavior of the composite. The unit-cylinder particles clearly strengthen the composite more than the other three shapes under a constant reinforcement fraction. This, however, does not imply that particles with sharp corners have a more pronounced strengthening effect, as shown by the case of “double-cone” particles, possessing the “sharpest” type of corners. A detailed analysis^[80] showed that the unit-cylinder and double-cone particles result in, respectively, the highest and lowest degrees of disturbance of the local plastic flow paths in the matrix. This directly reflects the different extents of constrained plastic flow and hence the strengthening behavior in the composite. Other simple unit-cell approaches focusing on various aspects of elastoplastic behavior of composites have been reported.^[8,77-90] In general, when the particle fraction is small, less than 0.2 for instance, the simple unit-cell approach presented above shows reasonably accurate results for the elastic response. At higher particle fractions the composite behavior will be dominated by the boundary conditions imposed on the unit cell, so care must be taken in interpreting the modeling result. The readers are referred to these references for detailed analyses, especially for the inelastic behavior. In some studies randomly distributed particles were also included in the computational model.^[91-93]

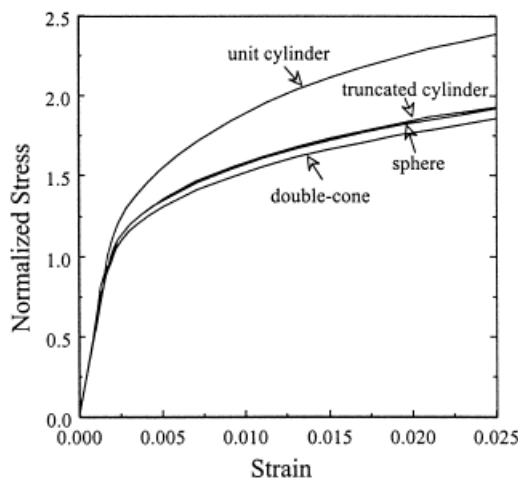


Fig. 10. Predicted tensile stress-strain curves for the Al/SiC/20_p composite with the various reinforcement shapes. The stress values are normalized by the matrix yield strength.

8. Deformation Behavior

In this section we focus on three aspects of composite deformation: thermal stress, creep behavior, and cyclic stress-strain response.

8.1. Thermal Stress

The thermal expansion mismatch between the reinforcement and the matrix results in thermal stresses within the composite upon cooling from the processing temperature to ambient temperature. As mentioned above, in actual composites thermal residual stresses are relieved by plastic deformation in the matrix, resulting in indirect strengthening.^[13] Figure 11 shows the calculated tensile stress-strain curves for 20% SiC reinforced Al alloy utilizing the unit-cylinder particles (Fig. 8a), with and without the presence of thermal residual stress. As before, the matrix was taken to be an isotropically hardening elastic-plastic material in the model. The thermal residual stresses were calculated for a composite cooled from the solutionizing temperature of 500 °C, where the composite is in a relatively stress-free state, to room temperature, 20 °C. Also included in the figure is the stress-strain response used for the pure matrix. During cooling the matrix at the particle/matrix interface undergoes yielding.^[77] This has direct bearing on subsequent loading of the material. It can be seen in Figure 11 that in the presence of thermal stresses a lower slope is observed at the early stage of deformation, due to the slightly lower apparent Young’s modulus arising from prior plastic deformation. When compared with the material free of residual stresses, higher values of the average axial stress were observed. This means that the existence of residual stresses enhances the initial strain hardening rate in the material. Comparing the curves for the pure matrix and for the composite without thermal residual stresses, direct strengthening effects are observed. The higher flow stress for the composite is a direct consequence of load transfer from the matrix to the reinforcement, which is also related to the

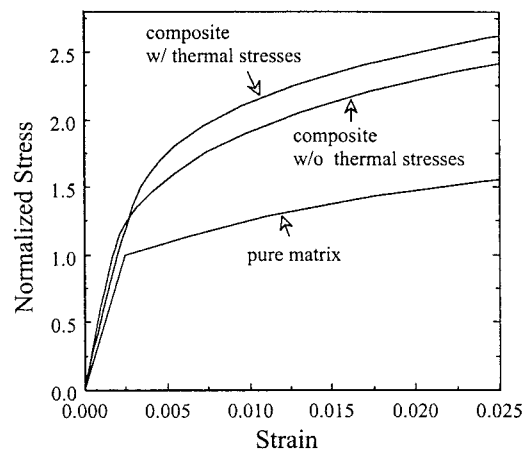


Fig. 11. Predicted tensile stress-strain curves of the Al/SiC/20_p composite, with and without the presence of thermal residual stresses. The predicted behavior of the Al matrix is also included and the stress values are normalized by the matrix yield strength.

constrained plastic flow within the matrix.^[80] A comparison of the two composite curves reveals the indirect strengthening effect. In the model strain hardening caused by cool down-induced plasticity leads to subsequent higher strength for the composite with thermal stresses incorporated (after the crossover point). In actual materials thermal mismatch-induced dislocation punching^[13] renders a higher matrix strength due to strain hardening. Thus, when appropriate constitutive models are chosen (e.g., hardening plasticity rather than perfect plasticity in the present case), continuum-based numerical modeling can provide insights into the deformation mechanisms. Direct comparisons of numerical modeling and experimental measurements of residual stresses in aluminum matrix composites have also been reported.^[95]

The ability to predict the coefficient of thermal expansion (CTE) of the composite is also quite important, particularly in applications where dimensional stability and the capability of matching the thermal expansion of other materials under thermal loading conditions is critical. The effective CTE of particle reinforced metal matrix composites, based on the known CTE values and elastic-plastic properties of the constituents, have been predicted. Shen et al.^[94] illustrated that the composite CTE is much less sensitive to variations in particle geometry than in the cases of elastic and plastic response. The effects of local plasticity and microvoids on the composite CTE have also been addressed along with experimental measurements.^[96-98]

8.2. Creep Behavior

A continuum-based unit-cell approach has also been used to model creep of metal matrix composites. Assuming a spherical particle and the power-law creep formulation for the metal matrix, Davis and Allison^[99] showed that the ratio of composite to matrix steady-state creep rates depends primarily on the volume fraction and geometry of the reinforcing phase, with the stress exponent of the composite and that of the matrix remaining relatively constant. A similar result was obtained for the case of rigid reinforcing particles.^[83] Dragon and Nix^[100] carried out similar analysis and obtained similar results for composites with aligned short fibers. The higher resistance to creep for the composite is largely attributed to the constrained matrix flow, leading to a reduced composite creep rate. More sophisticated aspects of creep deformation, such as interfacial slip, diffusion, and grain boundary sliding have also been included in some models (e.g., references^[101,102]). Since microstructural evolution cannot be easily accounted for in most finite element models, the anomalous behavior of stress exponent and activation energy described in previous sections cannot be easily studied numerically. By considering randomly oriented short fibers in the metal matrix, Dragon and Nix^[103] were able to predict the observed high values of stress exponent and activation energy found in

their materials. This treatment, however, applies only to certain classes of discontinuously reinforced MMCs.

8.3. Cyclic Stress-Strain Behavior

Characterizing the cyclic stress-strain behavior is one of the crucial steps toward understanding fatigue performance. In short-fiber reinforced composites,^[104] even when the matrix is assumed to exhibit isotropic hardening behavior (i.e., no Bauschinger effect exists), the composite shows a distinct Bauschinger effect upon reversed loading, as was observed experimentally.^[105] This was confirmed for particle reinforced composites,^[80] where it was demonstrated, through the examination of the evolution of local stress field, that the apparent early reversed yielding for the composite arises from the non-uniformity of deformation in matrix caused by the constraint imposed by the brittle reinforcement. Thus, high *local* effective stresses trigger early *local* yielding after the load is reversed, which is reflected in the macroscopic stress-strain behavior.

The above microplasticity effect in the composite is the same mechanism that causes the experimentally observed early deviation from linearity of the tensile stress-strain curve for metal matrix composites compared to the monolithic matrix material observed experimentally.^[17] This means that the *proportional limit* for the composite is actually lower than that of monolithic matrix material, although the composite shows a much higher macroscopic yield strength. Under cyclic loading, the lower proportional limit of the composite implies that, in a stress-controlled cyclic test with the stress range well within the elastic limit of the *unreinforced* material, the composite can actually develop a cyclic plasticity. This has been shown experimentally for the 2080/SiC_p-T8 composite.^[18] In order to adequately model the stabilized cyclic response without encountering elastic shake-down, in the modeling presented below kinematic hardening was assumed for the matrix with its elastic-plastic behavior taken from the experimental stress-strain behavior of the unreinforced Al alloy. Although the unit-cell model shown in Figure 8d was followed, a staggered distribution of particles was used to model the random orientation of particles.^[106,107]

Figure 12 shows the stabilized stress-strain response predicted by the staggered sphere model. The stress amplitude imposed is 350 MPa, which is well below the elastic limit of 489 MPa for the unreinforced alloy. Also included in the figure are the experimentally obtained stress-strain hysteresis loop. The predicted hysteresis loop is in extremely good agreement with the experiment. An examination of the deformation pattern in the computational domain reveals that localized plastic deformation occurs in the matrix even when the *overall* applied stress is well within the elastic range for the unreinforced matrix. Specifically, cyclic plasticity arises from plasticity at the poles of the reinforcement along the loading direction and adjacent to the reinforcement where the interface is roughly at 45° to the loading axis (maximum shear).

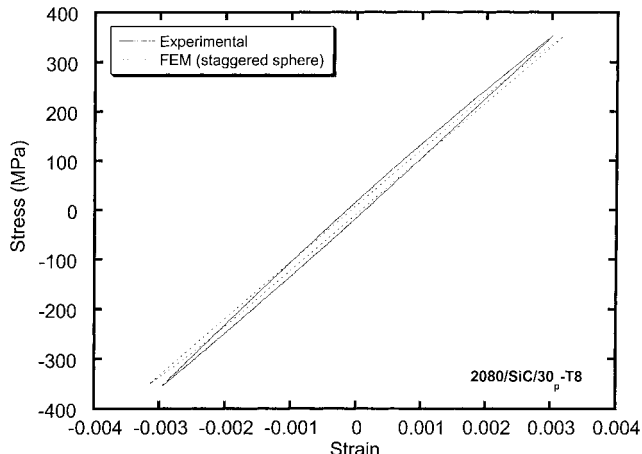


Fig. 12. Comparison of stabilized experimental and predicted cyclic stress-strain response for a Al/SiC/30_p composite.

It should be noted that our treatment of microplasticity or the Bauschinger effect in general is limited to the continuum assumption. If large deformation is involved in experiments, possible microstructural changes can then influence the cyclic response of the composite. For this discussion the reader is referred to Pragnell et al.^[108]

9. Damage Modeling

Modeling of damage in MMCs must take into consideration fracture of the ceramic reinforcement, void nucleation, growth and coalescence of voids within the metallic matrix, and/or decohesion and crack growth along the particle/matrix interface. Of these mechanisms fracture of the reinforcement particles is very important. In the remainder of this section, attention is devoted to the fracture of reinforcing particles in the composite.

Clearly, the other failure mechanisms are also important, although only a limited number of numerical studies have modeled matrix failure and interfacial effects.^[79,82,109,110]

Without invoking a damage model that can predict particle fracture *during* loading, the unit-cell models in Figure 8 can be employed to directly study the effects of particle cracking on composite properties. Here we consider the unit cylinder particle, with an existing crack, lying normal to the axis of the cylinder, cutting through the middle section of the SiC particle (i.e., spanning along the bottom side from the lower-left corner over a distance of r_0 in the models shown in Figure 8). The Al matrix and the interface are assumed to remain free of damage, although the changes in matrix fields due to the presence of the crack in the reinforcement are accounted for by the analysis. Thus the model represents an upper bound for particle damage (or lower bound for effective composite strength) wherein all the reinforcing particles in the composite are cracked.

Figure 13 shows the finite element predictions (denoted as "FEM: cracked particles") of the overall Young's modu-

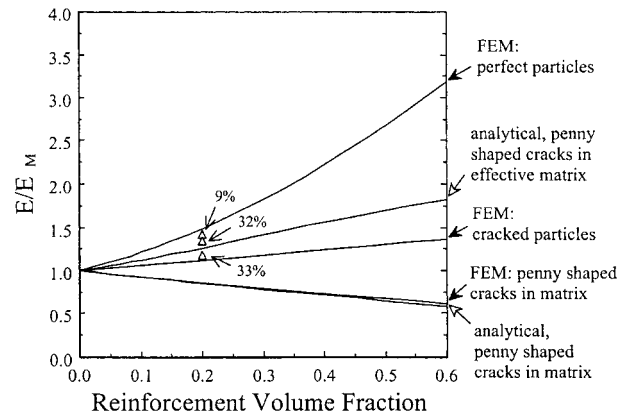


Fig. 13. Comparisons of the finite element predictions with the analytical bounds obtained from self-consistent estimates for the Al/SiC_p composite. Experimental results for the 20 vol. % reinforcement composite are shown by discrete data points where the numbers (in %) denote the fraction of broken particles.

lus (in the axial direction) of the composite as a function of the different fractions of cracked SiC particles. Also plotted for comparison purposes are the finite element predictions for the case where the particles remain intact (denoted as "FEM: perfect particles") and the case where the unreinforced matrix contains the same fraction of aligned, penny-shaped cracks as the fraction of the reinforcing particles (denoted as "FEM: penny-shaped cracks in matrix"). The former prediction for perfect particles represents the upper bound for maximum effective Young's modulus which can also be obtained from the simple treatment of elastic particles in an elastic matrix. The latter FEM predictions for the matrix cracking are in excellent agreement with the analytical prediction^[111] of the decrease in Young's modulus (in the direction normal to the crack plane) with increasing volume fraction of aligned penny-shaped cracks in the matrix alloy (denoted as "analytical," penny-shaped cracks in matrix). This analytical prediction represents the lower bound estimate for Young's modulus because it assumes that the cracked particles do not contribute to strengthening and may be considered as voids in the matrix of the composite.

The discrete points in Figure 13 show the experimentally measured elastic moduli for different fractions of fractured particles for the peakaged Al-3.5Cu matrix reinforced with 20 vol. % SiC particles.^[77,112] As expected, the experimental results fall within the bounds corresponding to the FEM predictions of particles for that volume fraction which are either fully intact or all fractured. The results of Figure 13 reveal that the overall elastic moduli of the Al/SiC_p composites, where all the SiC particles are fractured, are higher than those of the unreinforced matrix with a concentration of penny-shaped flaws equal to the concentration of the particles. This result implies that even when all the particles in the composite are fractured, the brittle particles contribute to stiffening and strengthening, so treating the cracked particle as a crack in the matrix (or a void for that matter) is not a valid assumption. In the case of Al/SiC_p

composites the ratio of reinforcement modulus to matrix modulus is about 6. It was found from a parametric analysis that for composites with this ratio equal to about 3, the enhancement in Young's modulus due to particle reinforcement will be offset by the reduction in Young's modulus due to particle fracture.^[77]

Similar calculations can be made for exploring the effects of particle fracture on the plastic response of the composite. Figure 14 shows the predicted tensile stress-strain curves with and without particle fracture for the same material above containing 20 vol.% unit cylinder particles. For cracked particles, two cases of crack length, a , were considered: $a = r_0$ and $a = 1.001 r_0$, the second case being that the crack has grown slightly into the matrix. The calculations were terminated at the fracture strain observed in the experiment. A drastic difference exists for the two cases of cracked particles, which was not the case for the elastic response of the composites. A detailed analysis can be found in reference^[112]. When the crack tip is at a small distance into the matrix rather than right at the particle-matrix interface, the overall stress carrying capability and work hardening decrease significantly. For comparison purposes, the experimental tensile curve is also shown in Figure 14. Near final failure, the experimental curve shows much lower work hardening and falls below the case of $a = r_0$ (assuming all particles have cracked), which suggests that, in practice, many cracks would grow into the matrix originating from particle fracture, and final failure by ductile linkage of existing cracks may take place. For other approaches devoted to various aspects of the progressive development of reinforcement damage, including analytical modeling, the reader may consult references^[112-120].

Received: November 09, 2000
Final version: January 11, 2001

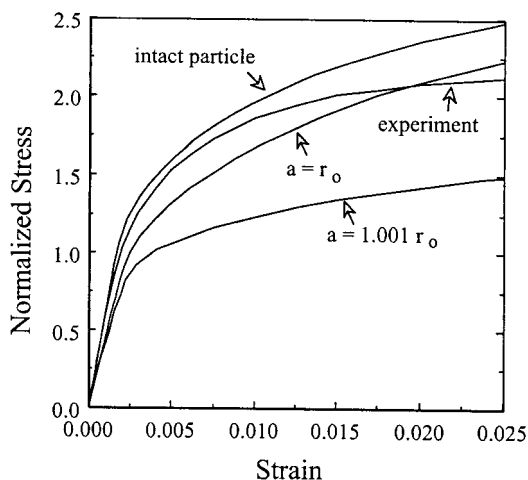


Fig. 14. Tensile stress-strain behavior of an Al/SiC/20_p composite obtained from experiments and from finite element calculations assuming: a) all particles are intact, b) right at the interface ($a = r_0$), and c) all particles are fractured with the crack tip protruding slightly into the matrix ($a = 1.001 r_0$). The stress values are normalized by the matrix yield strength.

References

- [1] K. K. Chawla, *Composite Materials - Science and Engineering*, 2nd Ed., Springer-Verlag, New York, 1997, 102.
- [2] T. W. Clyne, P. J. Withers, *An Introduction to Metal Matrix Composites*, Cambridge University Press, Cambridge, 1993, 1.
- [3] M. J. Koczak, S. C. Khatri, J. E. Allison, M. G. Bader, in *Fundamentals of Metal Matrix Composites*, (Eds. S. Suresh, A. Mortensen, A. Needleman), Butterworth-Heinemann, Stoneham, MA, 1993, 297.
- [4] B. Maruyama, W. H. Hunt, Jr., *J. Metals*, 1999, 51, 59 – 61.
- [5] H. L. Cox, *Brit. J. App. Phys.*, 1952, 3, 122.
- [6] A. Kelly, *Strong Solids*, Clarendon Press, Oxford, 1973, 157.
- [7] V. C. Nardone, K. M. Prewo, *Scripta Metall.*, 1989, 23, 291.
- [8] L. C. Davis, J. E. Allison, *Metall. Trans. A*, 1993, 24A, 2487.
- [9] N. Chawla, U. Habel, Y.-L. Shen, C. Andres, J. W. Jones, J. E. Allison, *Metall. Mater. Trans.*, 2000, 31A, 531–540.
- [10] K. K. Chawla, M. Metzger, *J. Mater. Sci.*, 1972, 7, 34.
- [11] K. K. Chawla, *Phil. Mag.*, 1973, 28, 401.
- [12] M. Vogelsang, R. J. Arsenault, R. M. Fisher, *Metall. Trans. A*, 1986, 17A, 379.
- [13] R. J. Arsenault, N. Shi, *Mater. Sci. Eng.*, 1986, 81, 175.
- [14] S. Suresh, K. K. Chawla, in *Fundamentals of Metal Matrix Composites*, (Eds. S. Suresh, A. Mortensen, A. Needleman), Butterworth-Heinemann, Stoneham, MA, 1993, 119.
- [15] P. E. Krajewski, J. E. Allison, J. W. Jones, *Metall. Mater. Trans.*, 1993, 24, 2731.
- [16] J. N. Goodier, *J. Appl. Mech.*, 1933, 55–7, 39.
- [17] S. F. Corbin, D. S. Wilkinson, *Acta Metall. Mater.*, 1994, 42, 1319.
- [18] N. Chawla, C. Andres, J. W. Jones, J. E. Allison, *Scripta Mater.*, 1998, 38, 1596.
- [19] N. Chawla, C. Andres, J. W. Jones, J. E. Allison, *Metall. Mater. Trans.*, 1998, 29A, 2843.
- [20] P. M. Mummery, B. Derby, D. J. Buttle, C. B. Scruby, in *Proc. of Euromat 91*, (Eds. T. W. Clyne, P. J. Withers), vol. 2, Cambridge, UK, 1991, 441–447.
- [21] M. Manoharan, J. J. Lewandowski, *Mater. Sci. Eng.*, 1992, A150, 179–186.
- [22] J. J. Lewandowski, D. S. Liu, C. Liu, *Scripta Metall.*, 1991, 25, 21.
- [23] S. Kamat, J. P. Hirth, R. Mehrabian, *Acta Metall.*, 1989, 37, 2395.
- [24] N. Chawla, J. J. Williams, G. Piotrowski, R. Saha, in *Proc. of Internat. Congress on Fracture ICF-10*, (Eds.: K. Ravichandran, R. O. Ritchie), 2001, in press.
- [25] F. A. Mohamed, K.-T. Park, E. J. Lavernia, *Mater. Sci. Eng.*, 1992, A150, 21–35.
- [26] T. G. Nieh, *Metall. Trans.*, 1984, 15A, 139–146.
- [27] D. Webster, *Metall. Mater. Trans.*, 1982, 13A, 1511–1519.
- [28] V. C. Nardone, J. R. Strife, *Metall. Trans.*, 1987, 18A, 109–114.

- [29] D. C. Dunand, B. Derby, in *Fundamentals of Metal Matrix Composites*, Butterworth-Heinemann, Boston, **1993**, 191–214.
- [30] Y. Li, T. G. Langdon, *Mater. Sci. Eng.*, **1999**, A265, 276–284.
- [31] P. W. Davies, G. Nelves, K. R. Williams, B. Wilshire, *Metal Sci. J.*, **1973**, 7, 87–92.
- [32] J. D. Parker, B. Wilshire, *Metal Sci. J.*, **1975**, 9, 248–252.
- [33] V. C. Nardone, J. K. Tien, *Scripta Mater.*, **1986**, 20, 797–802.
- [34] E. Artz, D. S. Wilkinson, *Acta Metall.*, **1986**, 34, 1893–1898.
- [35] B. Y. Zong, B. Derby, *Acta Mater.*, **1997**, 45, 41–49.
- [36] A. Kelly, W. R. Tyson, *J. Mech. Phys. Solids*, **1966**, 14, 177–186.
- [37] H. Lilholt, *Comp. Sci. Tech.*, **1985**, 22, 277–294.
- [38] M. Taya, H. Lilholt, in *Advances in Composite Materials and Structures* (Eds. S. S. Wang, Y. D. S. Rajapakse), ASME, New York, **1986**, 21–27.
- [39] K.-T. Park, E. J. Lavernia, F. A. Mohamed, *Acta Metall. Mater.*, **1990**, 38, 2149–2159.
- [40] Y. Li, T. G. Langdon, *Acta Mater.*, **1998**, 46, 1143–1155.
- [41] Y. Li, T. G. Langdon, *Mater. Sci. Eng.*, **1998**, A245, 1–9.
- [42] P. Yavari, F. A. Mohamed, T. G. Langdon, *Acta Metall.*, **1981**, 29, 1495.
- [43] N. Chawla, J. E. Allison, in *Encyclopedia of Materials: Science and Engineering*, Elsevier Press, **2001**, in press.
- [44] J. Llorca, *Prog. Mater. Sci.*, **2001**, in press.
- [45] J. J. Lewandowski, in *Comprehensive Composite Materials*, (Eds. A. Kelly, C. Zweben), vol. 3, Elsevier Press, **2000**, 151–187.
- [46] Y. Sugimura, S. Suresh, *Metall. Trans*, **1992**, 23A, 2231–42.
- [47] J. K. Shang, R. O. Ritchie, *Metall Trans.*, **1989**, 20A, 897–908.
- [48] D. L. Davidson, *Eng. Fract. Mech.*, **1989**, 33, 965.
- [49] D. M. Knowles, J. E. King, *Acta Metall. Mater.*, **1991**, 39, 793.
- [50] J. Hall, J. W. Jones, A. Sachdev, *Mater. Sci. Eng. A*, **1994**, A183, 69.
- [51] M. J. Couper, K. Xia, in *Metal Matrix Composites - Processing, Microstructure and Properties*, (Eds. N. Hansen et al.), Riso National Laboratory, Roskilde, Denmark, **1991**, 291.
- [52] G. M. Vyletel, D. C. Van Aken, J. E. Allison, *Scripta Metall. Mater.*, **1991**, 25, 2405–2410.
- [53] C. Calabrese, C. Laird, *Mater. Sci. Eng.*, **1974**, 13, 141–157.
- [54] C. Calabrese, C. Laird, *Mater. Sci. Eng.*, **1974**, 13, 159–174.
- [55] E. A. Starke, G. Luetjering, in *Fatigue and Microstructure*, (Eds. J. T. Stayley, E. A. Starke), American Society for Metals, **1979**, 205–243.
- [56] C. Li, F. Ellyin, *Mater. Sci. Eng. A*, **1996**, A214, 115.
- [57] M. Levin, B. Karlsson, *Int. J. Fatigue*, **1993**, 15, 377.
- [58] D. A. Lukasak, D. A. Koss, *Composites*, **1993**, 24, 262.
- [59] N. Chawla, C. Andres, L. C. Davis, J. W. Jones, J. E. Allison, *Metall. Mater. Trans.*, **2000**, 31A.
- [60] N. Chawla, J. W. Jones, J. E. Allison, in *Fatigue '99*, (Eds. X. R. Wu, Z. G. Wang), EMAS/HEP, **1999**.
- [61] R. M. Christensen, *Mechanics of Composite Materials*, Wiley, New York, **1979**.
- [62] Z. Hashin, *J. Appl. Mech.*, **1983**, 50, 481.
- [63] G. J. Dvorak, in *Metal Matrix Composites: Mechanisms and Properties* (Eds. R. K. Everett, R. J. Arsenault), Academic Press, Boston, **1991**, 1.
- [64] A. Needleman, S. R. Nutt, S. Suresh, V. Tvergaard, in *Fundamentals of Metal Matrix Composites*, (Eds. S. Suresh, A. Mortensen, A. Needleman), Butterworth-Heinemann, Boston, **1993**.
- [65] D. Francois, A. Pineau, A. Zaoui, *Mechanical Behavior of Materials, Volume I: Elasticity and Plasticity*, Kluwer Academic Publishers, Dordrecht, **1998**.
- [66] S. Suresh, A. Mortensen, *Fundamentals of Functionally Graded Materials*, IOM Communications Ltd, London, **1998**.
- [67] S. Nemat-Nasser, M. Hori, *Micromechanics: Overall Properties of Heterogeneous Materials*, North-Holland, Amsterdam, **1993**.
- [68] Z. Hashin, S. Shtrikman, *J. Mech. Phys. Solids*, **1963**, 11, 127.
- [69] J. D. Eshelby, *Proc. R. Soc. Lond. A*, **1957**, 241, 376.
- [70] T. Mura, *Micromechanics of Defects in Solids*, 2nd edition, Martinus Nijhoff, The Hague, **1987**.
- [71] E. Kroner, *Z. Phys.*, **1958**, 151, 504.
- [72] B. Budiansky, *J. Mech. Phys. Solids*, **1965**, 13, 223.
- [73] R. Hill, *J. Mech. Phys. Solids*, **1965**, 13, 213.
- [74] L. J. Walpole, *J. Mech. Phys. Solids*, **1966**, 14, 151.
- [75] T. Mori, K. Tanaka, *Acta Metall.*, **1973**, 21, 571.
- [76] O. B. Pedersen, *Acta Metall.*, **1983**, 31, 1795.
- [77] Y.-L. Shen, M. Finot, A. Needleman, S. Suresh, *Acta Metall. Mater.*, **1994**, 42, 77.
- [78] R. Saha, J. J. Williams, N. Chawla, unpublished work.
- [79] J. Llorca, S. Suresh, A. Needleman, *Metall. Trans. A*, **1992**, 23A, 919.
- [80] Y.-L. Shen, M. Finot, A. Needleman, S. Suresh, *Acta Metall. Mater.*, **1995**, 43, 1701.
- [81] T. Christman, A. Needleman, S. Suresh, *Acta Metall. Mater.*, **1989**, 37, 3029.
- [82] J. Llorca, A. Needleman, and S. Suresh, *Acta Metall. Mater.*, **1991**, 39, 2317.
- [83] G. Bao, J. W. Hutchinson, R. M. McMeeking, *Acta Metall. Mater.*, **1991**, 39, 1871.
- [84] C. L. Hom, *J. Mech. Phys. Solids*, **1992**, 40, 991.
- [85] G. L. Povirk, A. Needleman, S. R. Nutt, *Mater. Sci. Engng. A*, **1991**, 132, 31.
- [86] A. Levy, J. M. Papazian, *Acta Metall. Mater.*, **1991**, 39, 2255.
- [87] D. B. Zahl, R. M. McMeeking, *Acta Metall. Mater.*, **1991**, 39, 1117.
- [88] I. Dutta, J. D. Sims, D. M. Seigenthaler, *Acta Metall. Mater.*, **1993**, 41, 885.

- [89] E. Weissenbek, H. J. Bohm, F. G. Rammerstorfer, *Comput. Mater. Sci.*, **1994**, 3, 263.
- [90] D. Xu, S. Schmauder, E. Soppa, *Comput. Mater. Sci.*, **1999**, 15, 295.
- [91] N. J. Sorensen, S. Suresh, V. Tvergaard, A. Needleman, *Mater. Sci. Engng. A*, **1995**, 197, 1.
- [92] T. D. Papathanasiou, M. S. Ingber, L. A. Mondy, A. L. Graham, *J. Composite Mater.*, **1994**, 28, 288.
- [93] H. P. Ganser, F. D. Fischer, E. A. Werner, *Comput. Mater. Sci.*, **1998**, 11, 221.
- [94] Y.-L. Shen, A. Needleman, S. Suresh, *Metall. Mater. Trans. A*, **1994**, 25A, 839.
- [95] G. L. Povirk, M. G. Stout, M. Bourke, J. A. Goldstone, A. C. Lawson AC, M. Lovato, S. R. Macewen, S. R. Nutt, A. Needleman, *Acta Metall. Mater.*, **1992**, 40, 2391.
- [96] Y.-L. Shen, *Mater. Sci. Engng. A*, **1998**, 252, 269.
- [97] D. K. Balch, T. J. Fitzgerald, V. J. Michaud, A. Mortensen, Y.-L. Shen, S. Suresh, *Metall. Mater. Trans. A*, **1996**, 27A, 3700.
- [98] Y.-L. Shen, *Mater. Sci. Engng. A*, **1997**, 237, 102.
- [99] L. C. Davis, J. E. Allison, *Metall. Mater. Trans. A*, **1995**, 26A, 3081.
- [100] T. L. Dragon, W. D. Nix, *Acta Metall. Mater.*, **1990**, 38, 1941.
- [101] K. T. Kim, R. M. McMeeking, *Mech. Mater.*, **1995**, 20, 153.
- [102] S. B. Biner, *Acta Mater.*, **1996**, 44, 1813.
- [103] T. L. Dragon, W. D. Nix, *Acta Metall. Mater.*, **1992**, 40, 2781.
- [104] J. Llorca, A. Needleman, S. Suresh, *Scripta Metall. Mater.*, **1990**, 24, 1203.
- [105] R. J. Arsenault, S. B. Wu, *Mater. Sci. Engng.*, **1987**, 96, 77.
- [106] V. Tvergaard, *Acta Metall. Mater.*, **1990**, 38, 185.
- [107] M. Chaturvedi, Y.-L. Shen, *Acta Mater.*, **1998**, 46, 4287.
- [108] P. B. Pragnell, W. M. Stobbs, P. J. Withers, *Mater. Sci. Engng. A*, **1992**, 159, 51.
- [109] A. Needleman, S. R. Nutt, in *Advances in Fracture Research*, (Eds. K. Salama, K. Ravi-chandar, D. M. R. Taplin, P. Rama Rao), Pergamon, Oxford, **1989**, 2211.
- [110] A. Needleman, *Ultramicroscopy*, **1992**, 40, 203.
- [111] N. Laws, J. R. Brockenbrough, *Int. J. Solids Struct.*, **1987**, 23, 1247.
- [112] M. Finot, Y.-L. Shen, A. Needleman, S. Suresh, *Metall. Mater. Trans. A*, **1994**, 25A, 2403.
- [113] G. Bao, *Acta Metall. Mater.*, **1992**, 40, 2547.
- [114] V. Tvergaard, *J. Mech. Phys. Solids*, **1993**, 41, 1309.
- [115] C. A. Lewis, P. J. Withers, *Acta Metall. Mater.*, **1995**, 43, 3685.
- [116] J. Llorca, C. Gonzalez, *J. Mech. Phys. Solids*, **1998**, 46, 1.
- [117] L. C. Davis, C. Andres, J. E. Allison, *Mater. Sci. Engng.*, **1998**, A249, 40.
- [118] J. R. Brockenbrough, F. W. Zok, *Acta Metall. Mater.*, **1995**, 43, 11.
- [119] P. Poza, J. Llorca, *Metall. Mater. Trans. A*, **1999**, 30A, 869.
- [120] S. Ghosh, S. Moorthy, *Acta Mater.*, **1998**, 46, 965.
- [121] We follow the standard notation for metallic composites designated by the Aluminum Association. The matrix alloy is followed by the reinforcement composition. The latter is denoted as a particular reinforcement by the subscript "p". The volume fraction can also be introduced in this notation followed by the heat treatment, e.g. 2080 matrix reinforced with 20% SiC, peak-aged, would be denoted 2080/SiC/20_p-T6.